Experimental and analytical study on steel deck-glulam beam hybrid bridge behavior

KISS Lajos*, USUKI Seizo**, SASAKI Takanobu***

* M.Sc., Ph.D. student, Dept. of Civil Eng., Akita University, 1-1 Tegata, Gakuen-machi, Akita 010-8502
**Dr. Eng., Professor, Dept. of Civil Eng., Akita University, 1-1 Tegata, Gakuen-machi, Akita 010-8502
***Dr. Eng., Assistant Prof., Inst. of Wood Technology, Akita Pref. University, Noshiro 016-0876

The use of hybrid structures, that combine glued laminated timber (glulam) with steel, concrete or fiber reinforced plastic for increased strength, makes it possible to build more and more long-span timber bridges worldwide. The authors proposed the design of a glulam-steel hybrid bridge, with the intention of making timber bridge a more available option for short and medium span bridges. The authors subjected a bridge model to bending and failure tests in order to investigate the behavior of such hybrid structures and validate the composite beam theory used by the authors to design them. The tested model is composed of an orthotropic steel deck, attached to two double glulam beams, having rectangular cross sections. Vertically inserted glued-in steel ribs, one at the compression and two at the tension side, stiffen each beam. The deck is connected to the beams through the upper inserted steel ribs, which also act as shear connectors. Comparing the experimental results to the analytical ones proved the ability of the composite beam theory to describe the structural behavior of the tested model.

Keywords: glued laminated timber, orthotropic steel deck, failure test, failure mode

1. Introduction

New and old, modern and traditional: Japanese society is a living example that both of them can exist and work at the same time, together. Engineers in Japan and worldwide try to follow this direction and apply this way of thinking for example by combining glued laminated timber with traditional structural materials, such as steel, concrete or FRP[1] and build more and more long-span timber bridges. A recent example of steel-timber hybrid bridges is the Bōchu bridge[2),3)], built in Akita Prefecture, in 2001. Here, the glulam main girders are reinforced with vertically inserted steel ribs at the top and bottom surfaces. An orthotropic steel deck forms a hybrid structure with the girder, being welded to the upper inserted reinforcement. The Bōchu bridge has a length of 55.0 m with two continuous spans, achieved through four joints composed of field welding of the lower inserted steel reinforcements, as well as welding the deck plates. For bridges of this scale, this type of hybrid solution is preferred, because its simple structure is easy to design and build.

One condition to make this glulam-steel hybrid bridge structure more available and familiar for clients and bridge designers is to develop a comprehensible design method. The authors proposed the use of composite beam theory as a simple, but reliable way of design for this type of bridge. In order to validate the adaptability of this theory for the hybrid structure considered, experimental verification was necessary.

The above reason determined the authors to prepare a reduced scale model of an orthotropic steel deck-glulam beam hybrid bridge for short and medium span bridges, using Douglas fir glulam main beams and ⊥-shaped steel floor beams[4),5)]. In the last five decades Japanese cedar was widely planted in Japan because of its rapid maturation and usefulness in addition to its scent. While more and more cedars are planted each year, they are not effectively utilized. One step to stimulate the use of this material is to provide more engineering designs relying on cedar, such as the bridge in this paper, structure that uses Japanese cedar for its main and floor beams too, combined with a steel deck. The authors conducted nine bending tests and a failure test to investigate the structural response of this type of bridge. This paper presents the results of the failure test only, compared to the ones determined analytically by the composite beam theory. Among the included experimental and analytical results are strain distributions of main bridge components as well as deflections of them.

The effect of increasing the number of lower inserted steel ribs from one to two was also investigated. Experimental results show that they affect positively the structural behavior and failure mode of the steel-glulam hybrid bridge.

2. Bridge Description

2.1 Bridge Woodiness

The ratio of beam height versus span length is a very important aspect in the design of beam bridges. Choosing carefully this ratio to be comparable to ratios of other types of bridges helps making the timber bridge a viable option for bridge construction. The authors proposed a glued laminated timber and orthotropic steel deck hybrid beam bridge structure, for short and medium span bridges, using Douglas fir glulam main beams and ⊥-shaped steel floor beams, with a height-span ratio of h/L = 1/16[4),5)].

In order to give the steel-glulam hybrid structure a more timber bridge-like appearance and to use larger volume of domestic material, the authors decided to increase the area of visible timber surface. This was achieved by designing a similar bridge, but instead of using Douglas fir for main beams and steel for floor beams, Japanese cedar was considered as the material for both, resulting in a height-span ratio of h/L = 1/17[6)].

2.2 Bridge Prototype

The prototype structure consists of an orthotropic steel deck, attached to two double glulam main beams made of Japanese cedar. The orthotropic steel deck plate has a total length of 15.6 m (span is 15.0 m), a width of 6200 mm and a thickness of 12 mm. The deck plate is stiffened by eight U-shaped longitudinal ribs and seven double glulam floor beams of size 180x750 mm each, the latter being arranged with an interval of 2500 mm. The steel deck acts as the top flange of the main beams, having rectangular cross sections. The beam width of a single beam varies from 180 mm to 280 mm at near beam-ends, in order to overcome shear forces developed by reactive forces on the support[7)]. The beam depth remains constant, being equal to 900 mm.

The main beams are doubly reinforced by two sets of vertically inserted, glued-in steel ribs. The first set, applied on the compression side, consists of a single rib of a dimension of 10x 130 mm. The second set represents the tension reinforcement, consisting of two ribs, each having a cross section of 16x210 mm. After removing mill scale by sandblasting, these steel ribs are bonded by E6264D, an epoxy resin developed especially for steel-timber bridges.

The inserted steel rib on the compression side serves as shear connector between the deck and the main beams, while the role of the glued-in steel ribs on the tension side of the main beams is to compensate the longitudinal axial strength. Thus, a part of the steel deck (determined by the effective widths λ_1 = 715 mm and λ_2 = 1730 mm, obtained by applying the Japanese shear lag formula for roadway bridges), the upper and lower ribs and the double glulam main beam form a composite beam. Therefore the composite beam theory can be used to calculate the bending and shear stresses. As a summary, composite beam in this paper is defined as the hybrid structure within the width $\lambda_1 + c + \lambda_2$ (see Fig.1), structure which is compound of the double glulam main beam, inserted steel ribs and steel deck plate. The hybrid bridge structure discussed in this paper basically consists of two composite beams.

2.3 Bridge Model

The tested bridge structure is a reduced model (see Fig.1), being one-third the scale of the previously introduced prototype bridge. Thus, the total length of the orthotropic steel deck plate is reduced to 5.2 m (the span to 5.0 m), its width to 2067 mm and its thickness to t_d = 4.5 mm. The size of the seven double glulam floor beams becomes 60x250 mm each, arranged with an interval of 660 mm. The variation of the width of main beam takes place from b = 60 mm to 93.5 mm at near beam-ends. This happens on a length of 335 mm, taking a gradient of 1:10, since no other specification exists for it. The length of widened beam portion is 1015 mm (see Fig.5). The depth of main beam is h = 300 mm.

The cross section of widened main beam at support, together with an end floor beam is shown on the left side of Fig.1. The right side of the same figure shows the cross section of main beam at midspan and an intermediate floor beam.

The size of the vertically inserted ribs is also reduced. The compression reinforcement is a single rib of a dimension of 3x44 mm. The tension reinforcement consists of two ribs, each having a cross section of 6x70 mm. The effective widths of the steel deck become λ_1 = 239 mm and λ_2 = 577 mm.

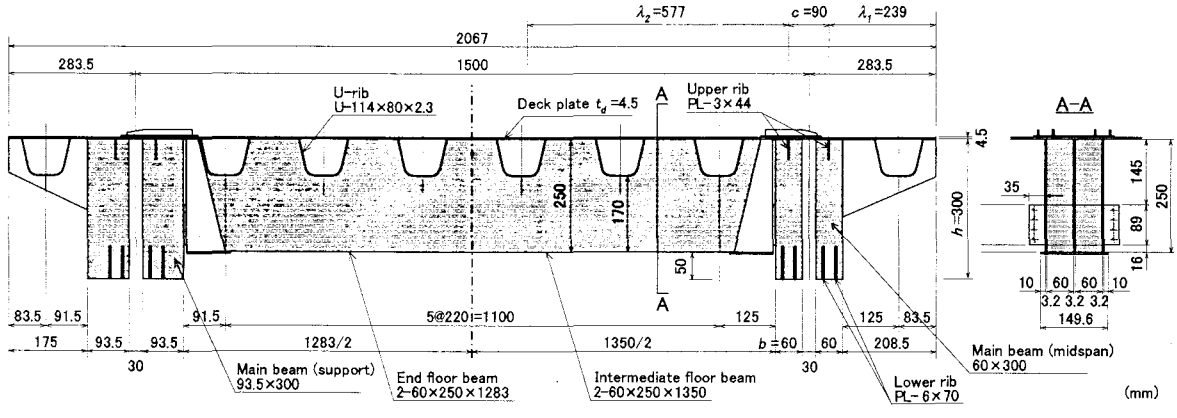

Fig. 1 Cross section of tested hybrid bridge model

2.4 Material Properties

The glued laminated timber material used for the reduced model was Japanese cedar of strength grade E75-F240 JAS (Japanese Agricultural Standard), while the steel material used for the inserted steel ribs as well for the orthotropic steel deck was SS400. An experimental value of bending moment capacity of Japanese cedar glulam was used for analytical calculations, being equal to $\sigma_{y,W}$ = 39 MPa. The experimental modulus of elasticity of Japanese cedar glulam is E_W = 9 GPa, the shear modulus is G_W = 601 MPa. The experimental yield strength $\sigma_{y,S}$ = 297 MPa and the allowable bending stress σ_{ba} = 137 MPa was used for SS400. The modulus of elasticity of steel equals E_S = 206 GPa.

3. Composite Beam Theory

As stated in 2.2, composite beam in this paper is defined as the hybrid structure within the width $\lambda_1 + c + \lambda_2$, compound of the double glulam main beam, inserted steel ribs and steel deck plate.

The bridge was designed using the concept of transformed section and converting all steel to an equivalent wood area[7]. In order to obtain this modified section, first the ratio of moduli of elasticity is calculated, being n = 23.

The authors used the plastic composite beam theory to determine the bending moments and loads corresponding to three main stages in the composite beam behavior. The first stage is when yielding of lower inserted steel ribs start: yield moment M_Y. Plastic moment M_P occurs when at mid-span, the cross section of lower inserted steel ribs is in fully plastic state. Determination of ultimate moment M_U is based on the assumption that failure of the composite beam takes place when tensile stress in the outer fibers of the double glulam main beam reaches the modulus of rupture of timber, i.e. $\sigma_x = \sigma_{y,W}$ = 39 MPa.

Analytical expressions of the above bending moments M_N (N = Y, P, U) are presented in a previous paper of the authors[5], while calculated values are as follows:

$$M_N = \begin{bmatrix} M_Y \\ M_P \\ M_U \end{bmatrix} = \begin{bmatrix} 143.9 \\ 180.6 \\ 245.4 \end{bmatrix} \text{kNm}$$

Numerical values of terms appearing in expressions of M_N are:

$$e_N = \begin{bmatrix} e_Y \\ e_P \\ e_U \end{bmatrix} = \begin{bmatrix} -69.7 \\ -76.0 \\ -92.8 \end{bmatrix} \text{mm}$$

$$\begin{bmatrix} A_S \\ A_P \end{bmatrix}_Y = \begin{bmatrix} 78.2 \\ 0 \end{bmatrix} \text{cm}^2 ; \quad \begin{bmatrix} A_S \\ A_P \end{bmatrix}_{P,U} = \begin{bmatrix} 61.4 \\ 16.8 \end{bmatrix} \text{cm}^2$$

$$\bar{I}_M = \int_{A_M} \bar{y}^2 dA \qquad (M = W, S) \tag{1}$$

$$\bar{I}_P = \frac{1}{2} A_P \left[(h - h_L)\left(\frac{h}{2} - h_L\right) - h_L e_P \right] \quad (\text{for } M_P) \tag{2}$$

$$\bar{I}_P = \frac{1}{2} A_P \left[h e_U + (h - h_L)\left(\frac{h}{2} - e_U\right) \right] \quad (\text{for } M_U) \tag{3}$$

$$\begin{bmatrix} \bar{I}_S \\ \bar{I}_P \end{bmatrix}_Y = \begin{bmatrix} 14.1 \\ 0 \end{bmatrix} \times 10^3 \text{ cm}^4$$

$$\begin{bmatrix} \bar{I}_S \\ \bar{I}_P \end{bmatrix}_P = \begin{bmatrix} 11.8 \\ 2.0 \end{bmatrix} \times 10^3 \text{ cm}^4 ; \quad \begin{bmatrix} \bar{I}_S \\ \bar{I}_P \end{bmatrix}_U = \begin{bmatrix} 11.8 \\ 2.4 \end{bmatrix} \times 10^3 \text{ cm}^4$$

where (as shown in Fig.2) e_N (N = Y, P, U) are the coordinates from the horizontal center line of double main beam to the neutral axis of composite beam for yield, plastic and ultimate bending moments, respectively; A_S is the cross section area of steel being in elastic state, i.e. deck plate and U-ribs within width $\lambda_1 + c + \lambda_2$ (see also Fig.1), upper ribs and (in function of $\bar{y}_P$) the lower ribs; A_P is the area of steel being in plastic state, i.e. (in function of $\bar{y}_P$) lower ribs; $\bar{I}_S$ and $\bar{I}_P$ are the moments of inertia for the previous steel areas, calculated with respect to the horizontal center line of double main beam; A_W = 341 cm^2 is the timber area of double main beam; $\bar{I}_W$ = 24.3 x 10^3 cm^4 is the elastic moment of inertia of timber of double main beam; h is the depth of main beam; h_L is the depth of lower ribs.

According to the loading scheme of the bending test, the loads acting on the composite beam, corresponding to M_N are:

$$R_N = \frac{2M_N}{\mu L} \qquad (N = Y, P, U) \tag{4}$$

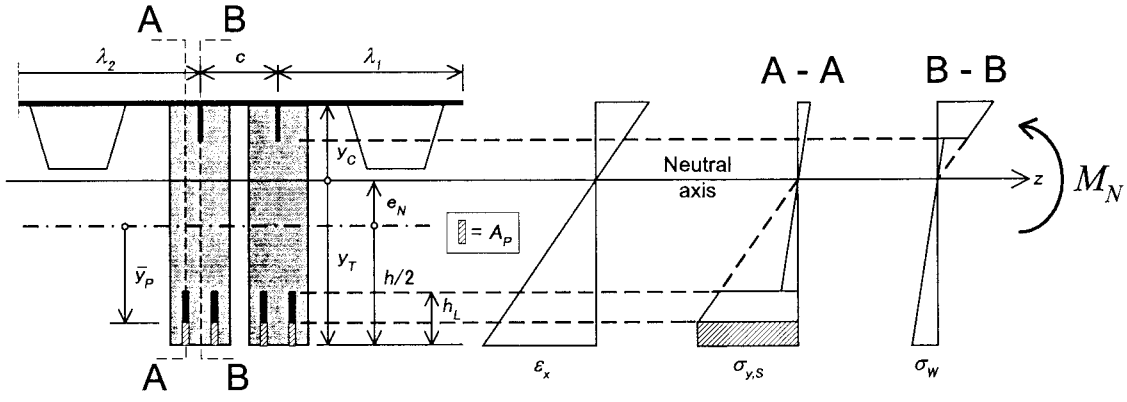

Fig. 2 Stress and strain distribution of elasto-plastic composite beam subjected to bending moments M_N (N = Y, P, U)

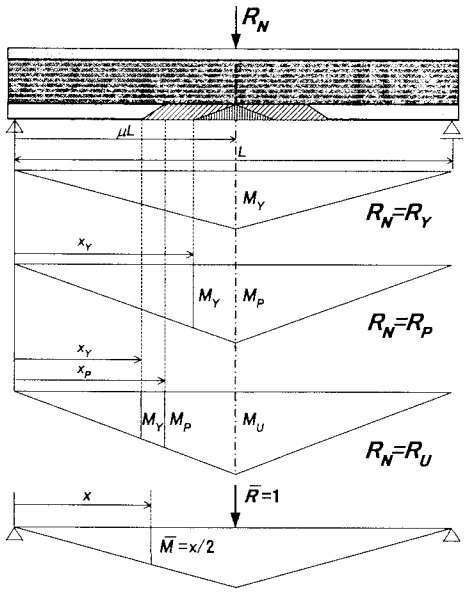

Fig. 3 Method of virtual work on elasto-plastic composite beam

where L is the bridge span; μL is the coordinate from the support to the cross section being under the applied load (μ = 0.5), as shown in Fig.3.

The mid-span deflections of the composite beam for bending moments M_N are expressed as follows:

$$\delta_Y = \frac{R_Y L^3}{48 E_W I_{V,Y}} \mu\left(3-4\mu^2\right) + \frac{\kappa R_Y \cdot \mu L}{2 G_W A_V} \tag{6}$$

$$\delta_P = \frac{M_P}{E_W}\left(\frac{x_Y^3}{3 I_{V,Y}\mu L} + \frac{1}{\mu L}\int_{x_Y}^{\mu L}\frac{x^2}{I_{V,P}}dx\right) + \frac{\kappa R_P \cdot \mu L}{2 G_W A_V} \tag{7}$$

$$\delta_U = \frac{M_U}{E_W}\left(\frac{x_Y^3}{3 I_{V,Y}\mu L} + \frac{1}{\mu L}\int_{x_Y}^{x_P}\frac{x^2}{I_{V,P}}dx + \frac{\mu^3 L^3 - x_P^3}{3 I_{V,U}\mu L}\right) + \frac{\kappa R_U \cdot \mu L}{2 G_W A_V} \tag{8}$$

where according to Fig.3 x_Y is the coordinate from the support to the cross section position where the bending moment is $M = M_Y$, used when $M_{max} \geq M_Y$; x_P is the coordinate of the cross section position where the bending moment is $M = M_P$, used in the case $M_{max} \geq M_P$; $I_{V,Y}$ is the elastic moment of inertia of the composite beam, used when $M \leq M_Y$; $I_{V,P}$ is the plastic moment of inertia of the composite beam, used in the case $M_Y \leq M \leq M_P$; $I_{V,U}$ is the ultimate moment of inertia of the composite beam, used when $M_P \leq M \leq M_U$. The moments of inertia $I_{V,N}$ (N = Y, P, U) are determined by the following expression:

$$I_{V,N} = \bar{I}_W + n\left(\bar{I}_S + \bar{I}_P\right) - e_N^2\left[A_W + n\left(A_S + A_P\right)\right] \tag{9}$$

having numerical values as listed below.

$$I_{V,N} = \begin{bmatrix} I_{V,Y} \\ I_{V,P} \\ I_{V,U} \end{bmatrix} = \begin{bmatrix} 244.3 \\ 218.1 \\ 165.8 \end{bmatrix} \times 10^3 \text{ cm}^4$$

In equations (6), (7) and (8) several constants are used, such as the equivalent cross section area of the composite beam[5]. This area has the value of A_V = 2138 cm^2. The other constant is the shear factor κ = 6.34 of the cross section[8].

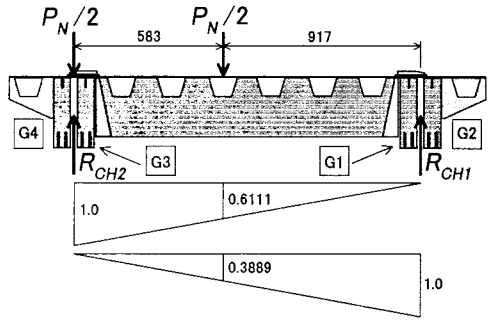

Fig. 4 Reactions on main beams due to applied load

Loads R_N determined by equation (4) are acting upon main beams G4 and G3 and correspond to R_{CH2} in Fig.4. In order to determine applied loads P_N (N = Y, P, U) on the whole structure, the above influence lines are used. Loads P_N are:

$$R_N = 1.0 \times P_N/2 + 0.6111 \times P_N/2$$
$$\Downarrow$$
$$P_N = R_N / 0.806$$

Numerical values of applied loads P_N corresponding to R_N (R_{CH2}) are shown in Table 1, together with the corresponding analytical deflections δ_N of main beams G4 and G3. Experimentally, the deflections of these beams are obtained by deflection meter CH2 (see Fig.5). Reactions R_{CH1} are calculated from loads P_N in order to obtain the deflections and strains of main beams G1 and G2.

Table 1 shows ratios of loads P_N versus allowable load P_A. The ratios P_N/P_A represent the safety factor for each assumed loading stage.

Table 1 Analytical loads and deflections

Case	P_N (kN)		δ_N (mm)		P_N/P_A
Allowable	P_A	56.7	δ_A	8.3	1.0
Yield	P_Y	142.9	δ_Y	20.7	2.5
Plastic	P_P	179.4	δ_P	27.0	3.2
Ultimate	P_U	243.7	δ_U	42.4	4.3

The value of allowable load P_A is established according to the Japanese Standard. For the bridge prototype, design bending moment M is calculated due to dead load, snow load and live load (T-loading: A live load) taking into account impact too (through impact factor i = 0.25). Then the value of the design bending moment for bridge prototype M = 1541 kNm at midspan is made equal to the bending moment corresponding to an equivalent static truck load acting on the structure. From this

equivalence the truck load $P_P = 4\,M/(1 + 0.6111)\,L$ is obtained (see the influence line in Fig.4). This pair of wheel loads includes the design dead load, snow load and live load with impact.

Reducing truck load P_P = 255 kN to the 1/3 scale model bridge (dividing both wheel loads by 9), loads denoted as $P_A/2$ are obtained. The equivalent static design load for the model bridge then will be equal to P_A = 56.7 kN (see Table 1), being the allowable load for this bridge model.

4. Failure Test Results with Discussion

The orthotropic steel deck-glulam beam hybrid bridge model was constructed, instrumented and tested to bending and failure at the structural testing laboratory of the Institute of Wood Technology, Akita Prefectural University, situated in Noshiro City, Japan. As stated earlier, prior to failure test the model was also subjected to nine bending tests, corresponding to nine loading cases. The difference between these cases (LC1 to LC9, see Fig.5) was the position of the applied truck wheel load. A load-controlled testing machine loaded the simply supported model. The failure test was performed at loading position LC2.

A total number of one hundred strain gauges (see Fig.5) were installed at four different cross sections along the hybrid bridge model. At sections A-A and B-B (appearing as A-A and

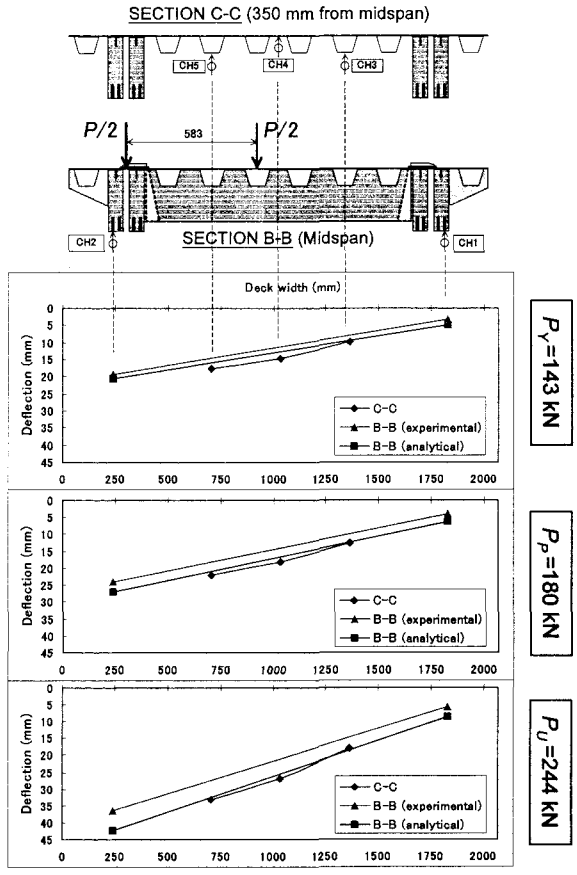

Fig. 6 Deflection of hybrid bridge model

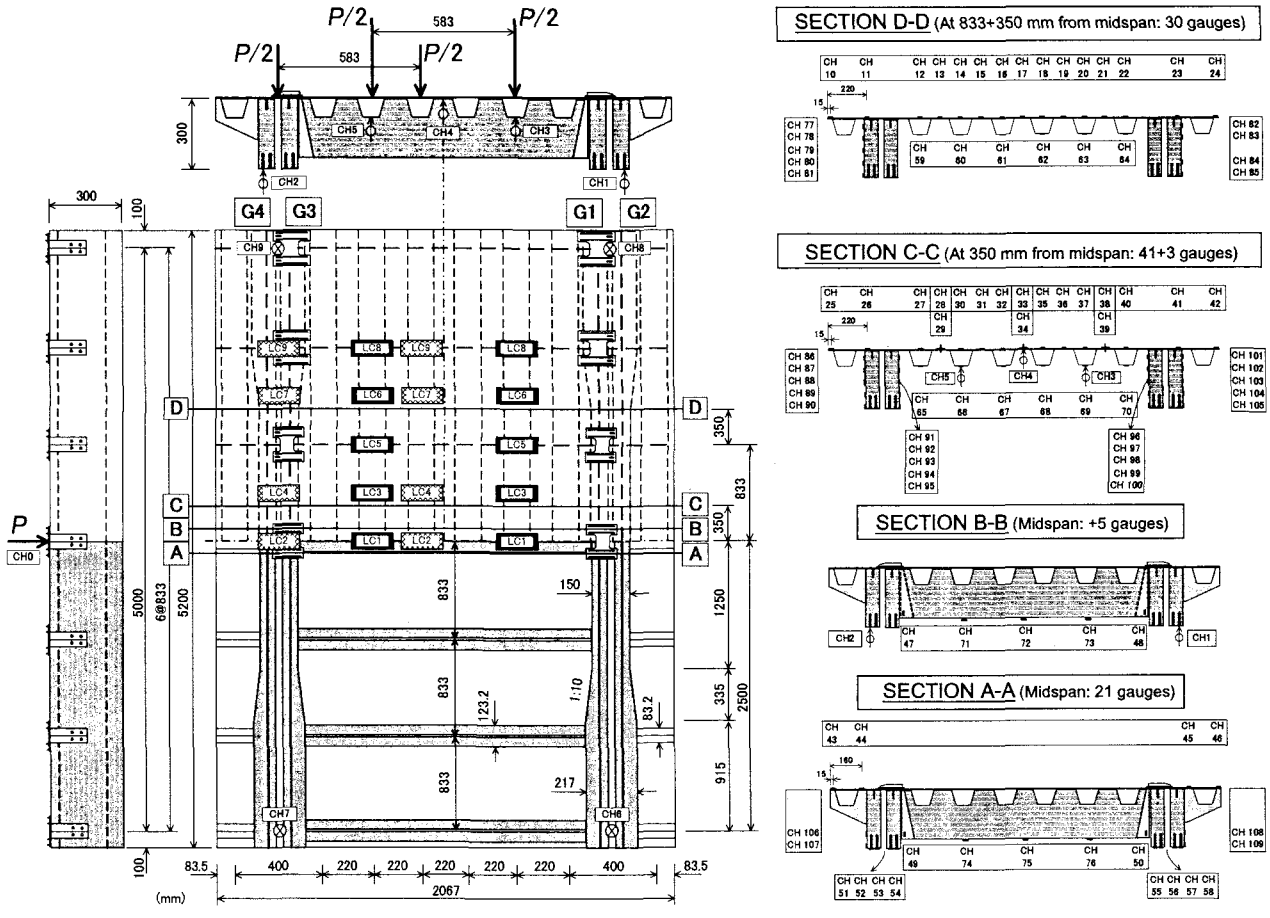

Fig. 5 Tested bridge model with all load cases, investigated sections and strain gauge positions

B-B in Fig.5 and Fig.7) gauges were installed to the bottom of floor beams, to steel side plates and to lower inserted ribs. At sections C-C and D-D (appearing as C-C and D-D in Fig.5 and Fig.7) gauges were applied along the depth of double glulam beams, on the upper surface of orthotropic steel deck and the bottom of U-ribs.

Fig.6 shows at loads P_m (m = Y, P, U) the deflection of U-ribs measured during failure test at section C-C by deflection meters CH3, CH4 and CH5, as well as deflection of main beams G4 and G2 measured at section B-B by deflection meters CH2 and CH1, respectively. For main beams at section B-B analytical deflection values are also included, closely following the experimental data.

Fig.8 gives a cross section view of the experimental and analytical strain distribution of the deck plate, U-rib, lower ribs, floor beam and side plates (for the position of gauges see Fig.5). The analytical strain distribution is given for deck plate, U-rib and lower ribs at analytical ultimate load P_U = 243.7 kN.

Distributions in Fig.8 are assumed to be uniform and limited by width $\lambda_1 + c + \lambda_2$ (Fig.1). Local deformation of deck plate near loading caused a non-uniform distribution (section C-C). Except this and the strain of lower ribs in main beams G4 and G3, all other experimental data follow closely the analytical predictions.

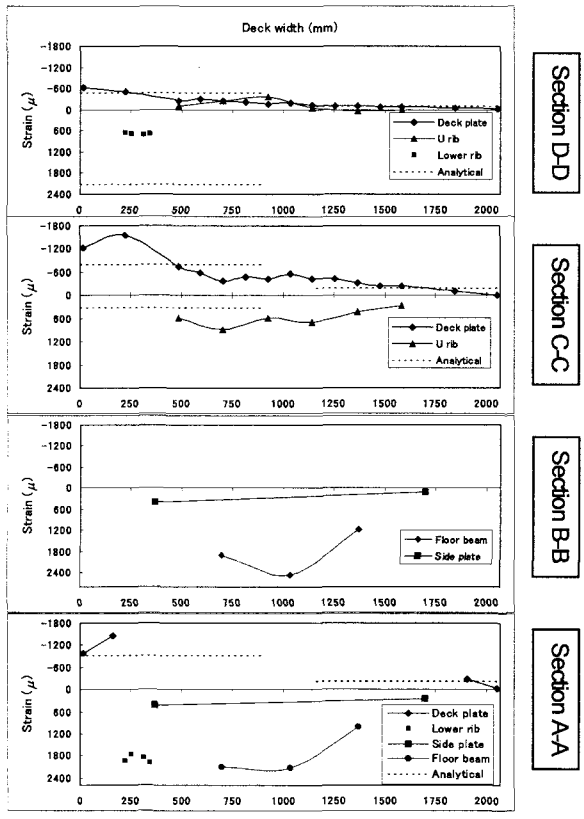

Fig. 8 Strain state of bridge members at P_U (section view)

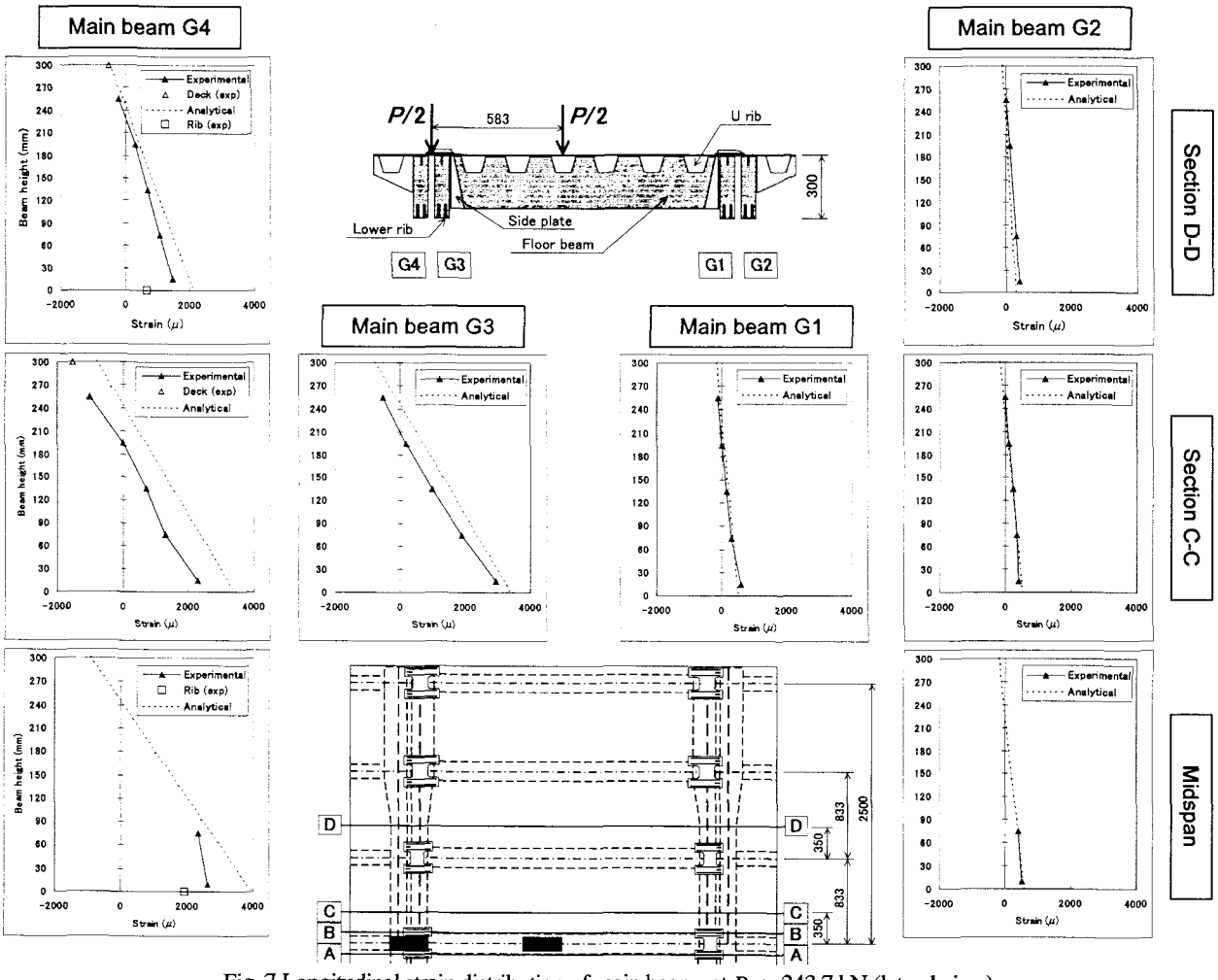

Fig. 7 Longitudinal strain distribution of main beams at P_U = 243.7 kN (lateral view)

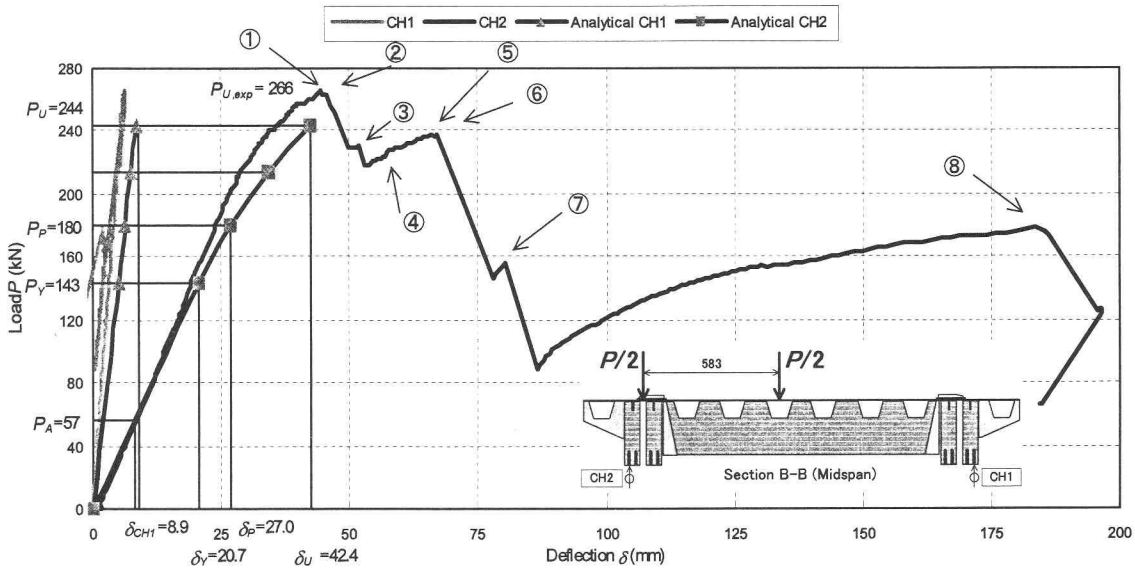

Fig. 9 Load-displacement curves at mid-span

The failure test was performed to validate the theoretical assumptions the authors used when applying the composite beam theory. Experimental curves of load P (applied at LC2) versus the deflections δ (measured by CH2 and CH1 at mid-span under main beams G4 and G2, respectively) are reported in Fig.9.

Drawing the analytical P-δ curves determined for CH2 and CH1 by the composite beam theory, we obtain curves that are very comparable to the measured ones. The experimental value of the ultimate load (failure load), corresponding to the ultimate bending moment is $P_{U,exp}$ = 266 kN. This value is about 9% higher than the analytical value of the ultimate load P_U = 243.7 kN, showing the ability of the composite beam theory to closely predict the structure failure load.

The failure of the model occurred in a ductile manner. Eight distinct failure positions were observed during the test (see failure positions ① to ⑧ in Fig.9), flexural failure starting from a knot situated at the tension side of beam G4. After failure position ⑦ the load-deflection curve rises again until failure position ⑧ due to the rigidity of the deck. Brittle failure with only one lower rib was observed in earlier tests[8),9)].

5. Conclusion

A reduced scale bridge model was subjected to failure test in order to investigate the structural behavior of steel-glulam hybrid bridges and to validate the applied composite beam theory. The analytically predicted failure load was only 9% less than the experimental one, thus proving the ability of the applied theory to effectively describe the behavior of this kind of structure.

Strain distributions of structural members are assumed to be uniform and limited by the effective widths of the steel deck: they are calculated for the width $\lambda_1 + c + \lambda_2$ (see Fig.1). Due to local deformation of deck plate near loading position, a non-uniform strain distribution was observed, peak values greatly differing from the predicted ones (section C-C). Except for this and the strain of lower ribs in main beams G4 and G3, all other experimental data follow closely the analytical predictions.

The main objective of the present research was to focus on the bending capacity of glulam main beams, not on the capacity of the steel deck plate. Even when the deck plate underwent local plastic deformations (see Fig.10), the main beams did not fail.

Fig.11 shows the P-δ curve of a previous test[4),5)] and of the failure test discussed in this paper.

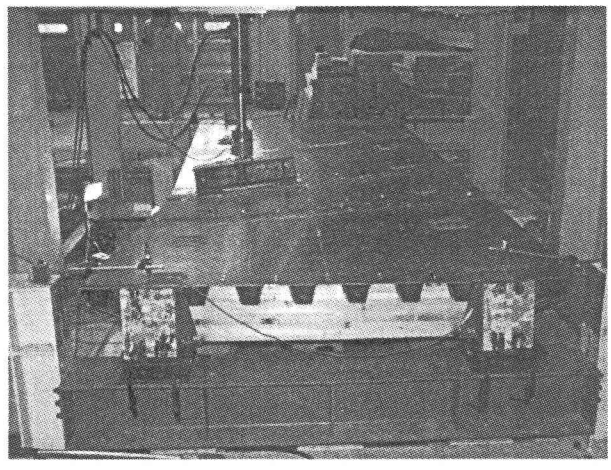

Fig. 10 Bridge model at failure

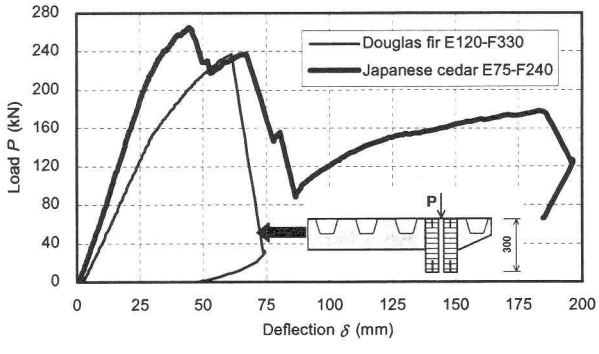

Fig. 11 Comparison of failure mechanisms

It can be observed the improvement in the failure mode of the Japanese cedar glulam-steel hybrid structure over the Douglas fir glulam-steel one, case when the failure of the hybrid structure occurred in a brittle manner. The authors consider the ductile failure to be the result of the increased steel reinforcement used at the tension side of the main glulam beams (double lower inserted ribs were used instead of single ones).

The authors plan to conduct a failure test on a structure exactly the same as the one in this paper, but applying the load at LC1. Results of this test will be presented in a future paper.

References

1) Bob, L., Gruin, A. and Kiss, L.: Alternative reinforcements of wooden beams, *Proceedings of IABSE Conference on Innovative Wooden Structures and Bridges*, pp.501-506, 2001

2) Usuki, S., Atsumi, A., Sudo, S. and Iijima, Y., A new timber beam bridge with an orthotropic steel deck, *Proceedings of the 6th World Conference on Timber Engineering*, pp.8.3.3-1 - 8.3.3-7, 2000

3) Usuki, S., Sasaki, T., Honda H., Iijima Y. and Atumi A., Field experiment of a hybrid timber-steel deck roadway bridge, *Proceedings of IABSE Conference on Innovative Wooden Structures and Bridges*, pp.181-186, 2001

4) Kiss, L., Usuki, S., Terada, H., Gotou, H. and Fujishima, E., Glued laminated timber and orthotropic steel deck hybrid beam: ultimate bending strength, *Proceedings of the 2nd Symposium on Timber Bridges*, pp.101-106, 2003

5) Kiss, L., Usuki, S. and Gotou, H., Experimental verification of ultimate bending strength of glulam-steel hybrid beam, *Journal of Structural Engineering, JSCE*, Vol. 50A, pp.891-896, 2004

6) Kiss, L., Usuki, S., Experimental study on load bearing capacity of steel deck-glulam beam hybrid bridge, *Proceedings of International Workshop on Resource Science and Engineering of Rare Metals*, pp.245-250, 2004

7) Usuki, S., Sasaki, T., Atsumi, A., Sharma, M.P.: Shearing stress of longitudinal rib plate of hybrid timber beam and orthotropic steel deck, *Journal of Structural Engineering, JSCE*, Vol. 47A, pp.1221-1227, 2001 (in Japanese)

8) Usuki, S., Gotou, H. and Kiss, L., Bending capacity of glued-laminated timber stiffened with inserted steel plate, *Journal of Structural Engineering, JSCE*, Vol. 49A, pp.889-894, 2003 (in Japanese)

9) Usuki, S., Sasaki, T., Gotou, H., Kiss, L., Ultimate strength of glulam sandwich beam reinforced by inserted steel ribs, *57th JSCE Annual Meeting*, I-366, 2002 (in Japanese).

(Received September 17, 2004)